Received: 26 March 2021 | Revised: 13 October 2021 | Accepted: 12 November 2021

DOI: 10.1002/cne.25275

RESEARCH ARTICLE

JCN RESEARCH IN SYSTEMS NEUROSCIENCE THE JOURNAL OF COMPARATIVE NEUROLOGY WILEY

Morphological and distributional properties of SMI-32 immunoreactive ganglion cells in the rat retina

Huiying Tan[1,2] | Xiaotao Li[1,3,4] | Kang Huang[1,2] | Moxuan Luo[1,5,6] | Liping Wang[1,2]

[1] Shenzhen Key Lab of Neuropsychiatric Modulation, Guangdong Provincial Key Laboratory of Brain Connectome and Behavior, CAS Center for Excellence in Brain Science and Intelligence Technology, Brain Cognition and Brain Disease Institute, Shenzhen-Hong Kong Institute of Brain Science-Shenzhen Fundamental Research Institutions, Shenzhen Institute of Advanced Technology, Chinese Academy of Sciences, Shenzhen, China

[2] University of Chinese Academy of Sciences, Beijing, China

[3] School of Biomedical Sciences, Li Ka Shing Faculty of MedicineThe University of Hong Kong, Hong Kong SAR, China

[4] Department of Brain and Cognitive Sciences, Massachusetts Institute of Technology, Cambridge, Massachusetts, USA

[5] University of Science and Technology of China, Hefei, China

[6] City University of Hong KongTat Chee AvenueKowloon, Hong Kong SAR, China

Correspondence
Liping Wang, Brain Cognition and Brain Disease Institute, Shenzhen Institute of Advanced Technology, Chinese Academy of Sciences, Shenzhen, 518055, China.
Email: lp.wang@siat.ac.cn

Huiying Tan and Xiaotao Li contributed equally to this study.

Funding information
Key-Area Research and Development Program of Guangdong Province, Grant/Award Number: 2018B030331001; National Natural Science Foundation of China, Grant/Award Number: 31930047; Natural Science Foundation of Guangdong Province, Grant/Award Number: 2018A030313439; National Natural Science

Abstract

SMI-32 is widely used to identify entire populations of alpha retinal ganglion cells (RGCs), and several SMI-32$^+$ RGC subsets have been studied thoroughly in rodents. However, due to the thick cover of SMI-32$^+$ neurofilaments, the morphology of SMI-32$^+$ RGCs in the central retinal region is obscured and rarely described. Moreover, SMI-32 labels more than one morphological RGC type and the full morphological characteristics and distribution of SMI-32$^+$ RGCs have yet to be discovered. Here, using intracellular neurobiotin injections combined with SMI-32 antibody staining, we investigated morphological and distributional properties of the entire SMI-32$^+$ RGCs population in the rat retina. We found that SMI-32$^+$ RGCs were evenly distributed throughout the rat retina. We compared the morphological features of SMI-32$^+$ ON and OFF cells in the central, middle, and peripheral retinal regions. We found that SMI-32$^+$ RGCs in different regions have distinct characteristics, such as the soma area and the dendritic field area, and Sholl analysis of ON cells and OFF cells revealed significant differences between each region. We classified SMI-32$^+$ RGCs into five clusters based on morphological features and found that a majority of SMI-32$^+$ RGCs belong to alpha-like cells; however, a small proportion of SMI-32$^+$ RGCs had small soma and small dendritic fields. Together, we present a full description of the morphology and distribution of SMI-32 immunoreactive RGCs in the rat retina.

KEYWORDS
alpha, classification, distribution, morphology, neurofilament, retinal ganglion cells, SMI-32

Foundation of China, Grant/Award Number: 31630031; Key Laboratory of Chinese Academy of Sciences, Grant/Award Number: 2019DP173024

1 | INTRODUCTION

Anti-SMI-32, a monoclonal antibody against the nonphosphorylated form of the neurofilament heavy protein (NFH; also known as NEFH), was first reported to label large Golgi type I neurons in the central nervous system (Ang et al., 1991; Campbell & Morrison, 1989; Sternberger & Sternberger, 1983). Since then it has subsequently been shown that anti-SMI-32 labels a group of large retinal ganglion cells (RGCs) in humans (Straznicky et al., 1992). The neurofibrillar staining method, modified from Gros–Schultze silver staining, was also shown to label alpha RGCs of the cat retina, which have a large soma and large dendritic arbors (Peichl & Wassle, 1981; Wassle et al., 1981a, 1981b). More recently, the SMI-32 antibody has been widely used to label whole populations of alpha RGCs (Baden et al., 2016; Bleckert et al., 2014; Lin et al., 2004; Schmidt et al., 2014; Sonoda et al., 2020).

The morphology and distribution of several SMI-32$^+$ RGCs subsets have been studied in detail in rodents, such as the ON-sustained RGC subset (Bleckert et al., 2014) and the melanopsin positive subset (Schmidt et al., 2014). However, a full description of the morphology and distribution of SMI-32$^+$ RGCs in the rat retina is still lacking. In particular, a description of those SMI-32$^+$ RGCs in the central retinal region is often obscured by SMI-32$^+$ neurofilaments. In addition, some studies have found evidence that SMI-32 labels are more than one type of RGC. A morphological study of the retina in C57BL/6 and Thy-1 (thymus cell antigen 1) transgenic mice indicated that the SMI-32 antibody is labeled at least four RGCs clusters, two of them with large somas and large dendritic fields as expected for alpha-like RGCs, whereas other clusters did not (Coombs et al., 2006). An investigation of physiological and morphological properties in C57BL/6J background transgenic mice revealed that SMI-32$^+$ RGCs produced ON-transient, ON-sustained, OFF-transient, and OFF-sustained responses (Krieger et al., 2017).

Here, we studied morphological and distributional properties of the entire populations of SMI-32$^+$ RGCs in the rat retina. We show that SMI-32$^+$ RGCs are evenly distributed throughout the rat retina. We describe morphological features of SMI-32$^+$ RGCs in the central, middle, and peripheral retinal regions and classify SMI-32$^+$ RGCs into five clusters based on morphological features. We also report that more than 90% of SMI-32$^+$ RGCs presented parvalbumin (PV) positive.

2 | MATERIALS AND METHODS

2.1 | Animals

All husbandry and experimental procedures in this study were in compliance with the standard of the Animal Care and Use Committees at the Shenzhen Institute of Advanced Technology, Chinese Academy of Sciences. Equal numbers of adult male and female (280–350 g) Sprague Dawley (SD) rats (Beijing Vital River Laboratory Animal Technology, Beijing, China) were used. Rats were housed at 22–25°C in a 12-h light/dark cycle environment with ad libitum access to food and water.

2.2 | Immunoperoxidase staining

Rats were deeply anesthetized with an intraperitoneal injection of sodium pentobarbital (80 mg/kg bodyweight). After eyes were enucleated, rats were sacrificed by cervical dislocation. Eyes were fixed in 4% paraformaldehyde (PFA) at 4°C overnight, and then transferred to 30% sucrose to equilibrate for 2 days at 4°C. After careful dissection, entire retinas were washed with phosphate buffer saline (PBS) 3 × 10 min, then rinsed in 1% H_2O_2 in PBS for 15 min, followed by three 10-min washes in PBS, then incubated in 0.3% Triton X-100 blocking solution with 10% goat serum for 1 h at room temperature. Retinas were then incubated in anti-SMI-32 antibody (Biolegend, Cat# 801702, Mouse, 1:1000, research resource identifiers (RRID): AB_2715852) overnight at 4°C. Following three 10-min washes in PBS, retinas were placed in a biotinylated mouse anti-mouse secondary antibody (Vector Laboratories, Cat# BA-9200, 1:200, RRID: AB_2336171) and reacted with 3-3′-diaminobenzidine (DAB) (DAB substrate kit; Vector Laboratories, Cat# SK-4100, diluted as the instruction). Finally, following another three 10-min PBS washes, retinas were mounted RGC-side up on microscope slides with coverslips. Images were acquired with a microscopy slide scanning system (Olympus VS120, Japan), and then SMI-32$^+$ cells were counted.

2.3 | Immunofluorescence staining

To stain the retina slices once fixed and equilibrated, eyes were embedded in Tissue-Tek OCT compound (Sakura Finetek; Japan) and stored at −20°C until sectioning. Superior-inferior axis and nasal-temporal axis sections crossing the optic disk were cut at a 20-μm thickness on a cryostat microtome (Lecia CM1950, Germany) and then mounted onto Super-Frost plus microscope slides (Fisherbrand; USA). Sections were rehydrated with PBS, permeabilized in 0.3% Triton X-100 in PBS containing blocking solution (10% goat serum) for 1 h at room temperature. Following this, the sections were incubated in the anti-SMI-32 antibody, mentioned above, overnight at 4°C. After gentle rinsing in PBS (3 × 10 min), the sections were incubated in secondary antibody (Alexa Fluor 594 or 488, Jackson ImmunoResearch, 1:200, RRID: AB_2338871, RRID: AB_2338840) for 2 h at room temperature and finally rinsed in PBS (3 × 10 min). Finally, the sections were embedded in a mounting medium with 4',6-diamidino-2-phenylindole (DAPI) (Vector Laboratories, USA) and gently covered with coverslips. Ten sections per retina were counted, and the average SMI-32$^+$ cell count from the central, middle, and peripheral regions of each retina was calculated.

TABLE 1 Primary antibody characterization

Antibody	Target	Immunogen	Host species	Supplier Catalogue	RRID	Concentration
SMI-32	Neurofilament H NF-H	Nonphosphorylated neurofilamentsfrom from rat brain separated by SDS-PAGE	Mouse	Biolegend Cat# 801702	AB_2715852	1:1000
Parvalbumin	Parvalbumin	Purified parvalbumin from rat skeletal muscle	Rabbit	Thermo Fisher Scientific Cat# PA1-933	AB_2173898	1:1000
Calretinin	Calretinin	Full length protein corresponding to Calretinin	Rabbit	Abcam Cat# ab702	AB_305702	1:1000
Melanopsin	Opsin 4	Synthetic peptide corresponding to residues K M(1) N S P S E S R V P S S L T Q D P S F(19) of rat melanopsin	Rabbit	Thermo Fisher Scientific Cat# PA1-780	AB_2267547	1:1000

For colabel staining, once fixed in PFA, entire retinas were dissected from eyecups in PBS and then washed in PBS (3 × 10 min). The retinas were then incubated in a blocking solution with 10% goat serum in 0.3% Triton X-100 and PBS for 1 h at room temperature, followed by incubation in anti-SMI-32 antibody overnight at 4°C, then placed in goat anti-mouse Alexa-488 conjugated IgG (Jackson ImmunoResearch, 1:200, RRID: AB_2338840) for 2 h at room temperature. Following this, the retinas were costained with another primary antibody (anti-PV, Thermo Fisher Scientific, Rabbit, Cat# PA1-933, 1:1000, RRID: AB_2173898; antimelanopsin, Thermo Fisher Scientific, Rabbit, Cat# PA1-780, 1:1000, RRID: AB_2267547; anticalretinin, Abcam, Rabbit, Cat# ab702, 1:1000, RRID: AB_305702). Finally, secondary antibody goat anti-rabbit Alexa-594 conjugated IgG (Jackson ImmunoResearch, 1:200, RRID: AB_2307325) was added to the retinas.

2.4 | Antibody characterization

Detailed information about each primary antibody used in this study is listed in Table 1. The SMI-32 antibody is a mouse monoclonal antibody made against a neurofilament heavy protein (200-220 kDa) (Sternberger & Sternberger, 1983). Immunostaining using this antibody allows the visualization of neuronal cell bodies, dendrites, and some thick axons in the central and peripheral nervous systems of humans and rodents (Ang et al., 1991; Campbell & Morrison, 1989; Peichl, 1989; Straznicky et al., 1992). The PV antibody is a polyclonal antibody raised in rabbits against skeletal muscle PV (12 kDa) from rats. Previous studies have reported that this antibody recognizes PV, but not other calcium-binding proteins (Condé et al., 1994). The calretinin antibody is a polyclonal antibody raised in rabbits by immunization with a full-length protein corresponding to calretinin (29 kDa). It recognizes calretinin in brain tissue of various animal species, but no staining is observed in the cerebellum of calretinin knockout mice (Schiffmann et al., 1999). The melanopsin antibody is a rabbit polyclonal antibody made against synthetic peptide corresponding to residues K M(1) N S P S E S R V P S S L T Q D P S F(19) of rat melanopsin (53 kDa for unglycosylated, 85 kDa for glycosylated). There is evidence that this antibody labels melanopsin protein specifically and has no reactivity in melanopsin knockout mice (Panda et al., 2002).

2.5 | Retina preparation and neurobiotin injections

Retinas were carefully yet rapidly dissected from eyecups in 95% O_2/5% CO_2 bicarbonate buffered artificial cerebrospinal fluid (ACSF), which contained (in mM): 125 NaCl, 25 $NaHCO_3$, 10 glucose, 2.5 KCl, 1.3 NaH_2PO_4, 1.3 Na-ascorbate, 0.6 Na-pyruvate, 2 $CaCl_2$, 1.3 $MgCl_2$ (pH 7.35 when saturated with 95% O_2/5% CO_2 at room temperature). Isolated retinas were mounted RGC-side up on filter paper (GS, 0.22 mm; Millipore Corp., Bedford, MA, USA) with a 1-mm^2 window cut on the center and kept in oxygenated ACSF at room temperature prior to filling with neurobiotin.

The mounted retinas were then set in an injection chamber and perfused with oxygenated ACSF continually at a fixed rate (0.5 mL/min). Individual cells were visualized using an upright fixed-stage microscope (FN-S2N; Nikon, Japan). SMI-32-like RGCs (with large somas) were targeted under the control of a micromanipulator (MP-225, Sutter Instruments, USA). Recording pipettes were formed by a micropipette puller (PC-10, Narishige, Japan) with a tip resistance of 6–7 mΩ and filled with internal solution (in mM): 130 K gluconate, 1 EGTA, 10 NaCl, 10 HEPES, 2 $MgCl_2$, 0.133 $CaCl_2$, 3.5 Mg-ATP, 1 Na-GTP with 0.5% neurobiotin (Vector Laboratories, Burlingame, CA, USA, Cat# SP-1120). Cells were voltage-clamped in whole-cell mode with a MultiClamp700B amplifier (Molecular Devices, USA), and pipettes were removed after a 5-min diffusion of neurobiotin internal solution. Retinas were incubated for another 5 min in the chamber to allow the soma and dendrites to be completely filled and stained. After completion of the neurobiotin injection, the retinas were incubated in 4% PFA for 1 h at room temperature, followed by three 10 min washes in PBS and blocking incubation in 10% goat serum for 1 h. Retinas were then incubated in Alexa Fluor 488-conjugated streptavidin (Molecular Probes, Cat# S32354, 1:200,

RRID: AB_2315383) for 4–6 h at room temperature and washed in PBS (3 × 10 min). Neurobiotin completely filled RGCs were costained with anti-SMI-32 antibody. Confirmed SMI-32$^+$ RGCs were then imaged for further data collection.

2.6 | Microscopy and morphometry

SMI-32$^+$ RGCs were imaged using confocal microscopy (LMS880, Zeiss, Germany). Z-stacks images of the whole morphology of individual RGC were acquired and then combined into a single maximum brightness projection image using ImageJ (National Institutes of Health, Bethesda, MD). The *Simple Neurite Tracer* Image J plug-in was used to manually trace the dendritic arbor of each cell, and the rendered paths images were generated as previously described (Iaboni et al., 2020). Parameters were measured as follows—(1) soma area: area of cell body; (2) diameter of soma: the longest diameter of cell body; (3) dendritic field area: the area made from joining the ends of each terminal dendritic branch together using straight lines; (4) arbor asymmetry: the distance between the center of mass of dendritic density and the cell body position; (5) total branches: total number of branches; (6) total dendritic length: the sum of the length of all branches. The soma area, diameter of soma, and dendritic field were calculated using the ImageJ "measure" function. Asymmetry, number of branches, and total dendritic length were calculated based on the rendered paths image. Sholl analysis was performed on the rendered paths image generated above with the Sholl *analysis* ImageJ plug-in as described before (Ferreira et al., 2014).

2.7 | Cluster analysis

To classify the SMI-32$^+$ RGCs, we performed unsupervised clustering based on the six measured parameters, including ON OFF property, soma area, dendritic field area, arbor asymmetry, total branches, and total dendritic length. Clustering was implemented with custom MATLAB (The MathWorks Inc, Natick, MA) scripts and the built-in hierarchical clustering function (MATLAB Statistics Toolbox). Before clustering, each parameter was normalized by the *z*-score method using the following equation:

$$z_i = \frac{x_i - \bar{x}}{\sigma} \quad (1)$$

where x_i is the *i*th RGC sample's parameter, $\bar{x}$ is the mean value of x, σ is the standard deviation of x, and z_i represents the *z*-scored value of x_i. Then, the *z*-scored values of all the six parameters were used to calculate the paired-wise distance matrix of the 83 SMI-32$^+$ RGCs with the Euclidean distance metric. Based on this distance matrix, we used Ward's method to calculate linkage distances between the different groups of cells. Finally, 83 SMI-32$^+$ RGCs were classified into five clusters using the iterative agglomerative procedure.

2.8 | Statistical analysis

All data were analyzed by using the GraphPad Prism 8.0 software (GraphPad, USA). Results are shown as mean ± standard error of mean (SEM). The unpaired student's *t*-test was used for two groups comparison and one-way ANOVA for three or more groups. Asterisks indicate the level of statistical significance (*p<.05; **p<.01; ***p<.001).

3 | RESULTS

3.1 | SMI-32$^+$ RGCs are evenly distributed throughout the rat retina

The SMI-32 antibody has been widely used to identify alpha RGCs and subsets of SMI-32$^+$ RGCs have been studied thoroughly (Bleckert et al., 2014; Okigawa et al., 2020; Schmidt et al., 2014; Sonoda et al., 2020). The RGC ON-sustained subset, which can be labeled with SMI-32, was reported to display a nasal-to-temporal gradient in cell density (Bleckert et al., 2014). Melanopsin-positive SMI-32$^+$ RGCs were reported to be distributed evenly throughout the retina (Schmidt et al., 2014). However, the distribution of the entire population of SMI-32$^+$ RGCs in rats still needs further confirmation. Therefore, we performed DAB staining on whole-mounted retinas (Figure 1a). SMI-32$^+$ RGCs in the periphery of each quadrant, including the superior-temporal (ST), inferior-temporal (IT), inferior-nasal (IN), and the superior-nasal (SN), were counted (Figure 1b). We found that SMI-32$^+$ RGCs were distributed evenly in four quadrants with a density of approximately 130 cells per square millimeter (ST: 130.80 ± 13.75; IT: 127.10 ± 15.43; IN: 132.10 ± 15.65; SN: 127.00 ± 12.91) (Figure 1c). Due to a thick cover of SMI-32$^+$ neurofilaments, we failed to measure the density of SMI-32 RGCs in the middle and central parts of the retina precisely. So, we stained sections crossing the optic disk and calculated SMI-32$^+$ RGCs in the center, middle, and periphery (Figure 1d) and found that SMI-32$^+$ RGCs were distributed evenly in every region of the rat retina (Figure 1e).

3.2 | Basic morphological features of SMI-32$^+$ RGCs

The dendrite architecture is an essential foundation for the physiological RGC function. There is evidence that the shape of RGC dendrites determines how visual information is received and integrated (Lefebvre et al., 2015; Liu & Sanes, 2017). To reveal the whole morphology of individual SMI-32$^+$ RGCs, we injected neurobiotin intracellularly into each SMI-32$^+$ RGC-like cell in each region of the retina. To ensure randomness in sampling, we divided each retina into four equal parts; for each part, we randomly injected one SMI-32-like cell in each region (central, middle, and peripheral) (Figure 2a). A total of 112 RGCs were filled, and 83 were confirmed SMI-32 positive by immunofluorescence staining (Figure 2b). Morphological feature analysis was based on these 83 SMI-32$^+$ cells (for statistics, see Table 2). Consistent with previous work (Coombs et al., 2006), we found that SMI-32 not only labels large alpha cells but also those with diameters smaller than 20 μm with small dendritic field area (Table 2). In these 83 SMI-32$^+$ RGCs, linear regression analysis showed

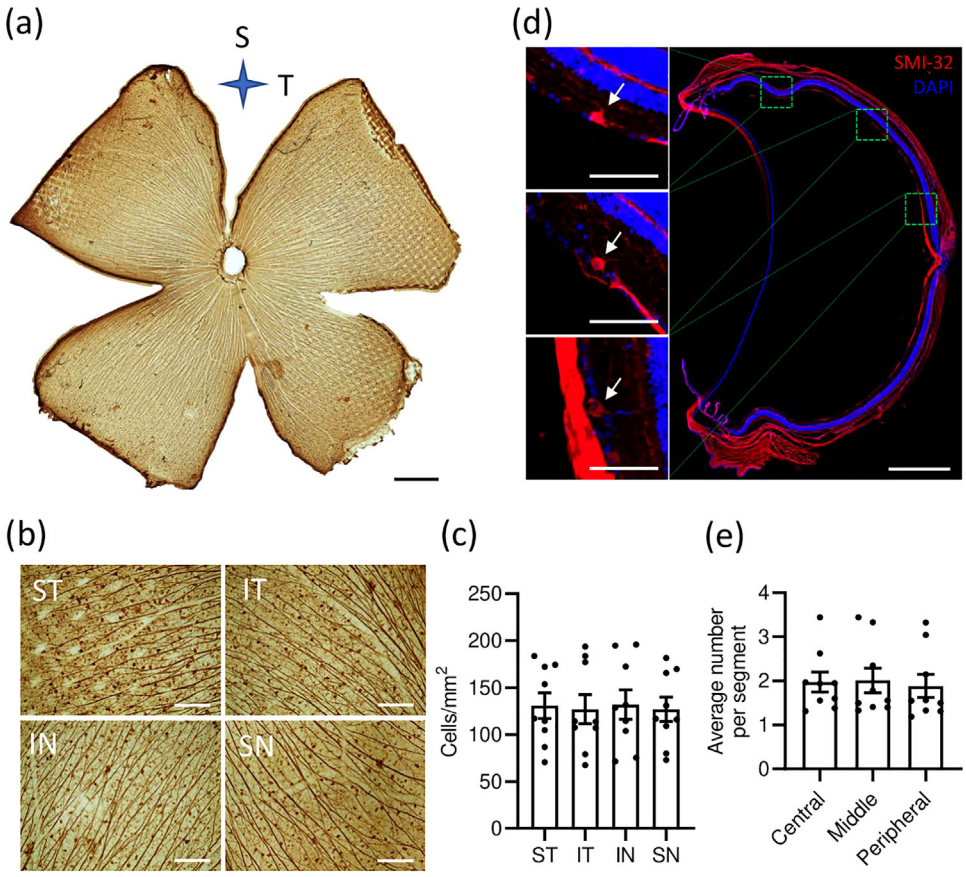

FIGURE 1 SMI-32$^+$ RGCs are evenly distributed throughout the rat retina. (a) DAB staining of the whole-mounted rat retina. Scale bar = 1 mm. (b) DAB staining of four quadrants. Scale bar = 300 μm. (c) Bar graph showing RGC counts in the four quadrants following DAB staining (n = 9 retinas/group, data presented as mean ± SEM). (d) Immunofluorescence staining of SMI-32 antibody (red) on retinal section. Scale bar = 1 mm (right), scale bar = 100 μm (left). (e) Bar graph showing of SMI-32$^+$ cell counts in three retinal regions following antibody immunofluorescence staining (n = 9 retinas/group, data presented as mean ± SEM)

TABLE 2 Morphological parameters of all 83 neurobiotin-filled SMI-32$^+$ RGCs

	Diameter of soma (μm)	n	ON, OFF			Soma area (mean ± SEM, μm^2)	Dendritic field area (mean ± SEM, 10^3 μm^2)	Total dendritic length (mean ± SEM, mm)
			ON	OFF	ON-OFF			
Central	<20	4	1	3	–	192.41 ± 19.50	81.57 ± 6.54	4.56 ± 0.49
	20–30	13	6	5	2	353.35 ± 28.43	155.40 ± 17.85	6.54 ± 0.72
	≥30	9	5	4	–	530.02 ± 25.18	151.39 ± 26.99	6.18 ± 0.45
Middle	<20	4	3	1	–	157.92 ± 25.58	81.20 ± 15.63	4.92 ± 0.21
	20–30	14	3	11	–	338.08 ± 20.28	102.62 ± 7.62	5.39 ± 0.30
	≥30	10	5	5	–	521.51 ± 21.18	146.71 ± 12.72	6.82 ± 0.35
Peripheral	<20	3	2	1	–	239.91 ± 12.38	98.60 ± 6.79	5.94 ± 0.72
	20–30	16	9	5	2	385.24 ± 20.59	153.79 ± 17.11	5.87 ± 0.28
	≥30	10	3	7	–	543.19 ± 37.27	173.19 ± 17.92	7.71 ± 0.37

that soma area was positively correlated with dendritic field area (r^2 = .1047; Figure 2c), in addition to total dendritic length (r^2 = .1686; Figure 2d).

To further investigate different characteristics in different parts of the retina, we compared SMI-32$^+$ RGCs between the central, middle, and peripheral regions and also between ON cells and OFF cells (ON–OFF cells were not included). We found that in the central retina, both the soma area (Figure 2e) and the dendritic field area (Figure 2f) of ON cells were larger than that of OFF cells, but not in the middle or peripheral retinal regions. The dendritic field area of OFF cells at the

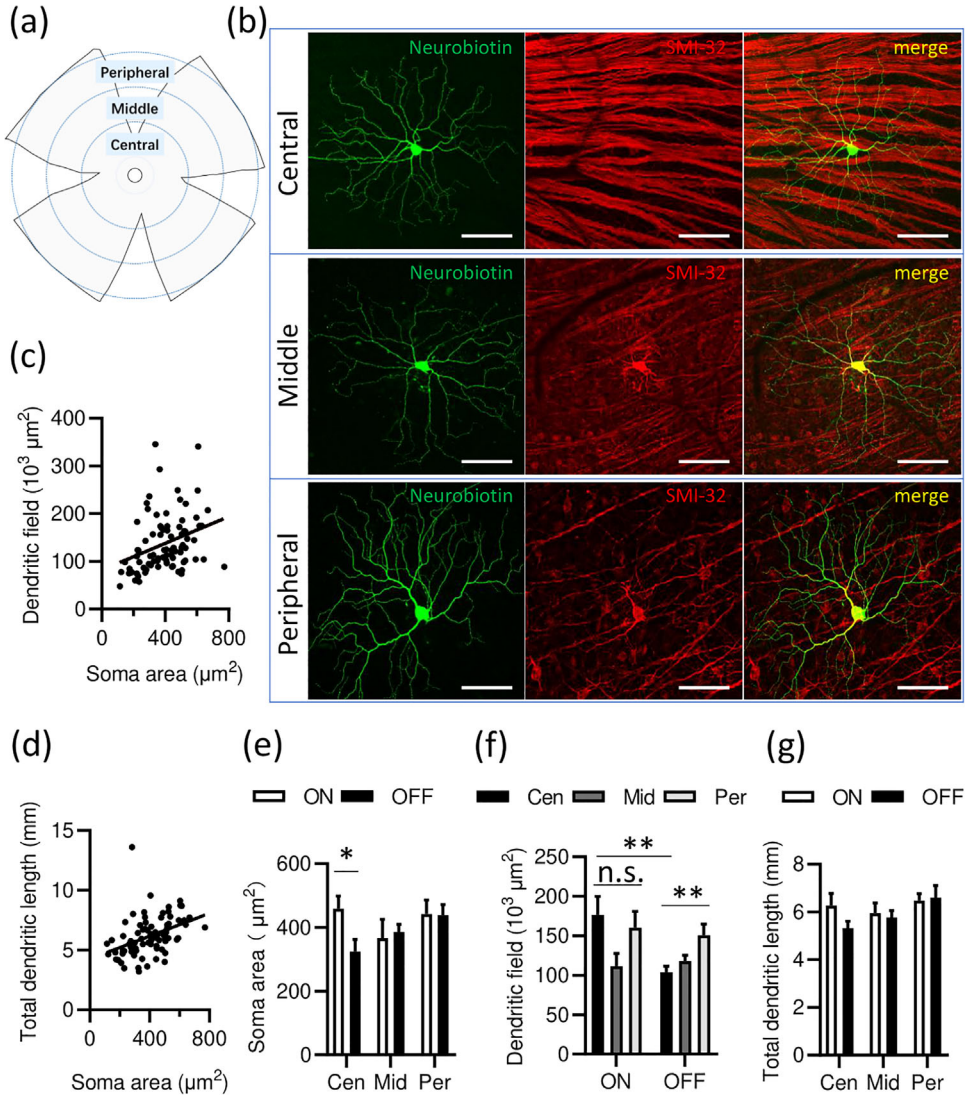

FIGURE 2 Basic morphological features of SMI-32$^+$ RGCs. (a) Diagram showing different retinal regions. (b) Neurobiotin-filled RGCs (green) costained with SMI-32 antibody (red) in each retinal region. Scale bar = 100 μm. (c) Linear regression analysis between soma area and dendritic field area (r^2 = .1047). (d) Linear regression analysis between soma area and total dendritic length (r^2 = .1686). (e) Soma area, (f) Dendritic field area, (g) total dendritic length (n = 12 for central (Cen) ON cells, n = 11 for middle (Mid) ON cells, n = 14 for peripheral (Per) ON cells, n = 12 for central OFF cells, n = 17 for middle OFF cells, n = 13 for peripheral OFF cells; data presented as mean ± SEM; unpaired student's t-test; $^*p$ <.05; $^{**}p$ <.01)

periphery was larger than at the center, a pattern not observed in ON cells (Figure 2f). There was no significant difference between total dendritic length between different retinal regions or between ON and OFF cells (Figure 2g).

3.3 | Arbor asymmetry of SMI-32$^+$ RGCs

Arbor asymmetry refers to the distance between the center of mass of dendritic density and the position of the cell body (Bae et al., 2018; Ran et al., 2020). We measured all 83 neurobiotin-filled SMI-32$^+$ RGCs and found that arbor asymmetry ranged approximately from 0 to 100. Arbor asymmetry was not significantly correlated with the soma area (r^2 = .0009401; Figure 3a), and there was no significant difference in arbor asymmetry between different retinal regions, nor between ON and OFF cells (ON-OFF cells not included; Figure 3b). Furthermore, both ON cells and OFF cells were distributed in each arbor asymmetry interval (Figure 3c,d). These results suggest that subsets of SMI-32$^+$ RGCs may have both symmetric and asymmetric arbor morphologies.

3.4 | Sholl analysis of SMI-32$^+$ ON and OFF cells

The Sholl analysis, a well-known technique was first used to describe the dendritic organization of cortical cat neurons (Sholl, 1953). More recently, it has also been widely applied to the quantitative analysis of RGC dendritic complexity (Bird & Cuntz, 2019; Bleckert et al., 2014; Iaboni et al., 2020). We used a 10-μm radius step size to generate

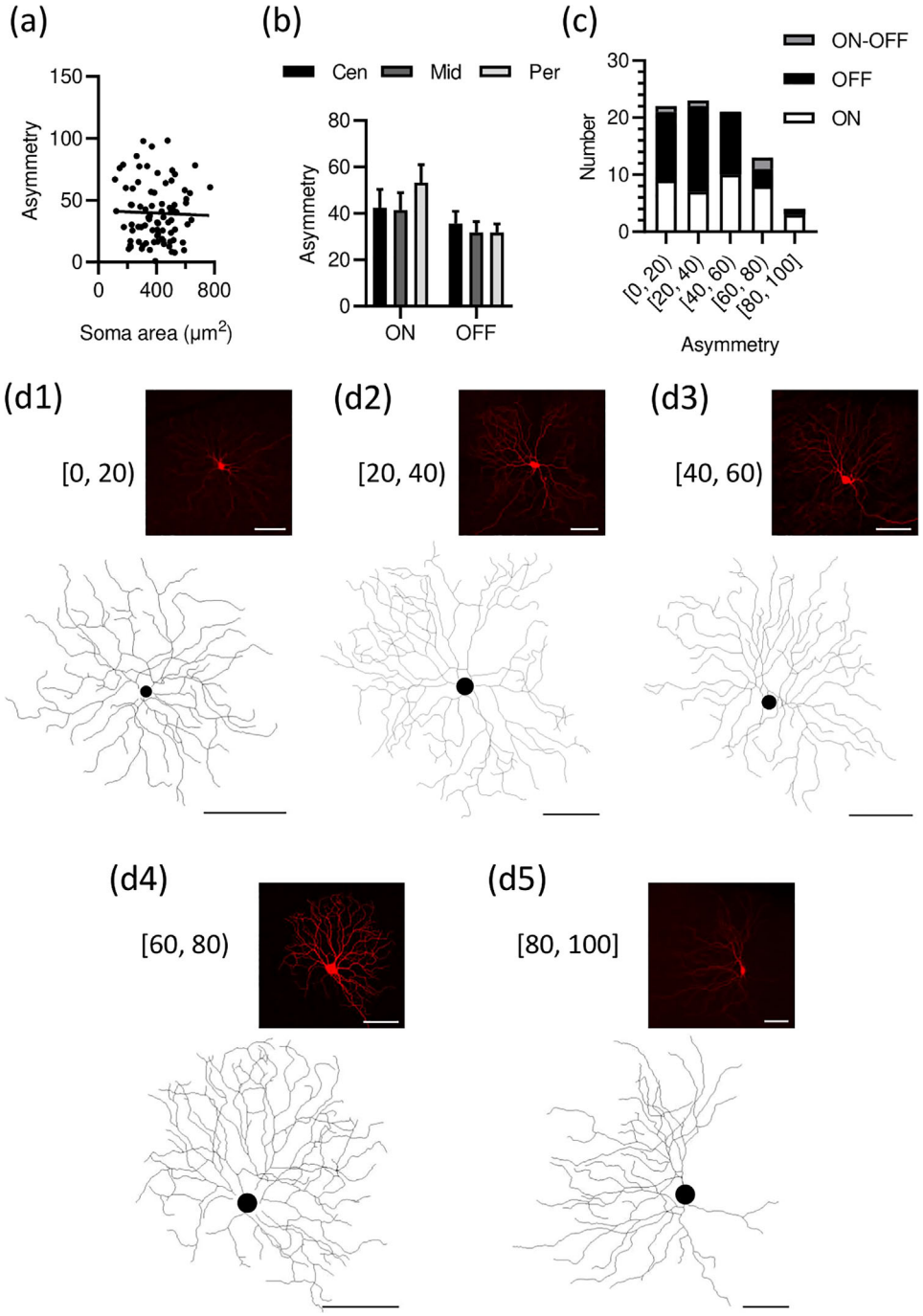

FIGURE 3 Arbor asymmetry of SMI-32$^+$ RGCs. (a) Linear regression analysis between soma area and arbor asymmetry (r^2 = .0009401). (b) Arbor asymmetry (n = 12 for central (Cen) ON cells, n = 11 for middle (Mid) ON cells, n = 14 for peripheral (Per) ON cells, n = 12 for central OFF cells, n = 17 for middle OFF cells, n = 13 for peripheral OFF cells; data presented as mean ± SEM). (c) Number of cells in each interval (n = 22 for [0, 20), n = 23 for [20, 40), n = 21 for [40, 60), n = 13 for [60, 80), n = 4 for [80, 100]). (d) Morphology of cells in each interval, (d1) for [0, 20), (d2) for [20, 40), (d3) for [40, 60), (d4) for [60, 80), (d5) for [80, 100]. Scale bar = 100 μm

gradually increasing concentric circles from the soma center (Figure 4a). The number of dendrite intersections with each concentric circle was calculated. We performed Sholl analysis on SMI-32$^+$ RGCs (ON-OFF cells not included) filled with neurobiotin. We found that the distance from the soma center to the highest branch density radius was significantly longer in ON cells than in OFF cells in each part of the retina (Figure 4c), but not significantly different at maximum branch density (Figure 4b). The number of intersections with each radius in ON and OFF cells in each retinal area was calculated using the area under the curve statistical approach (Figure 4d). These results indicate that SMI-32$^+$ ON and OFF cells have different dendritic structures, which perhaps reflect differences in physiological function.

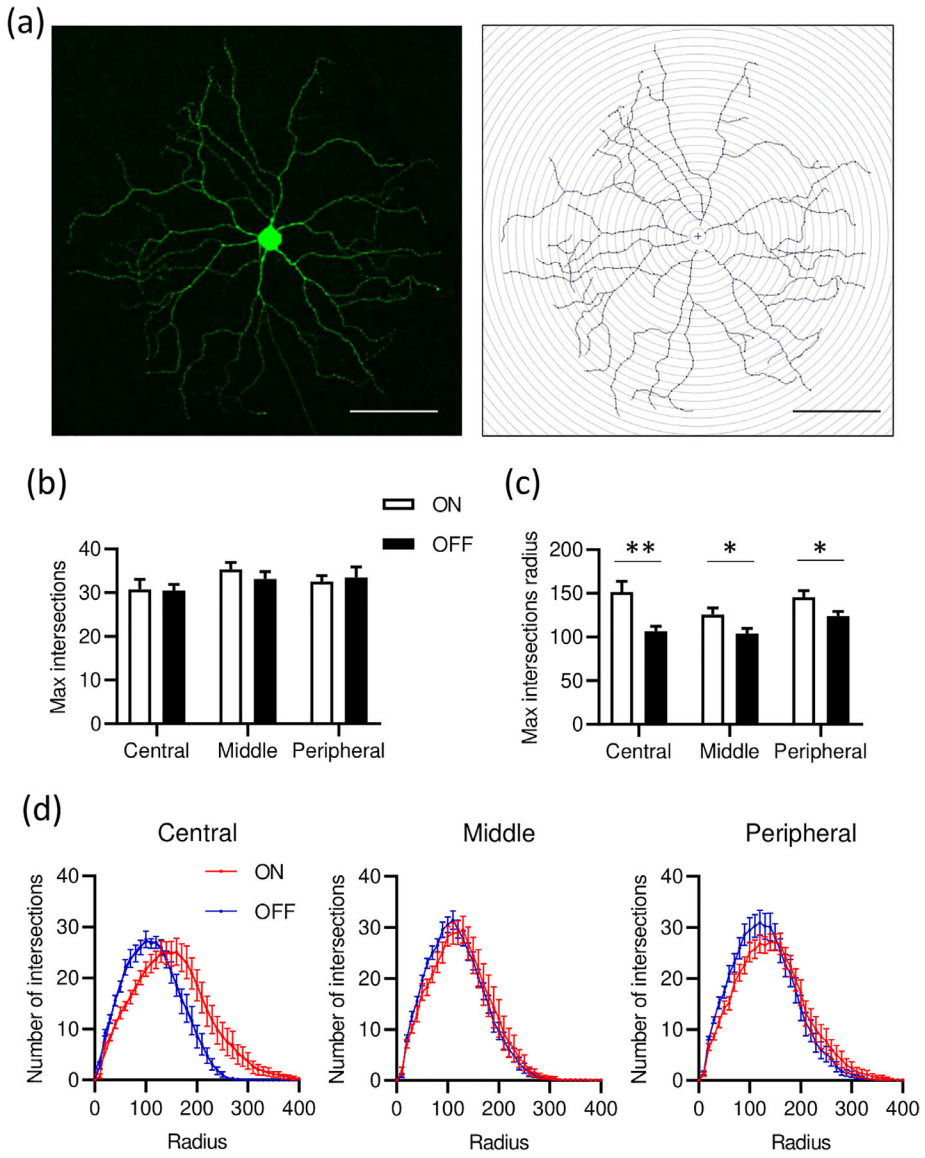

FIGURE 4 Sholl analysis of SMI-32$^+$ ON and OFF cells. (a) Demonstration of Sholl analysis: a neurobiotin-filled cell (left), and Sholl analysis of the cell (right). Scale bar = 100 μm. (b) Maximum intersections, reflecting the highest number of branches in the arbor. (c) Maximum intersections radius, reflecting sites of highest branch density (unpaired student's *t*-test; *p<.05; **p<.01). (d) The number of intersections in each retinal region and the area under the curve (for all graphs, n = 12 for central ON cells, n = 11 for middle ON cells, n = 14 for peripheral ON cells, n = 12 for central OFF cells, n = 17 for middle OFF cells, n = 13 for peripheral OFF cells; data presented as mean ± SEM)

3.5 | Classification of SMI-32$^+$ RGCs into five clusters

Consistent with previous reports (Coombs et al., 2006; Krieger et al., 2017), our results show that SMI-32 antibodies recognized more than one type of RGC morphology (Table 2). Here, we classified SMI-32$^+$ RGCs based on morphological features. We performed a hierarchical cluster analysis on all 83 neurobiotin-filled SMI-32$^+$ RGCs. Six parameters were used for the analysis: ON OFF property, soma area, dendritic field area, arbor asymmetry, total branches, and total dendritic length. Our results suggest that it was suitable to classify these SMI-32$^+$ RGCs into five clusters (Figure 5a). Each cluster included both ON cells and OFF cells (Figure 5b). In Figure 5c,d,e, among the five clusters, cluster 2 has the smallest soma area and dendritic field area, and the shortest total dendritic length, which does not match the morphological features of alpha RGCs (Krieger et al., 2017; Peichl, 1989, 1991). Cluster 1 has relatively medium soma area and dendritic field area, and total dendritic length. Cluster 3 has the largest soma area, dendritic field area, and the longest total dendritic length. The soma area of clusters 4 and 5 is somewhere between cluster 1 and cluster 3, but the dendritic field area and total dendritic length were not significantly different between clusters 3–5. Consistent with the inference in Figure 3, there was no consistency in arbor asymmetry among five clusters (Figure 5f). The morphology of representative cells in each cluster is shown in Figure 5g using the same scale. For a summary of the morphological parameters of the five clusters, see Table 3.

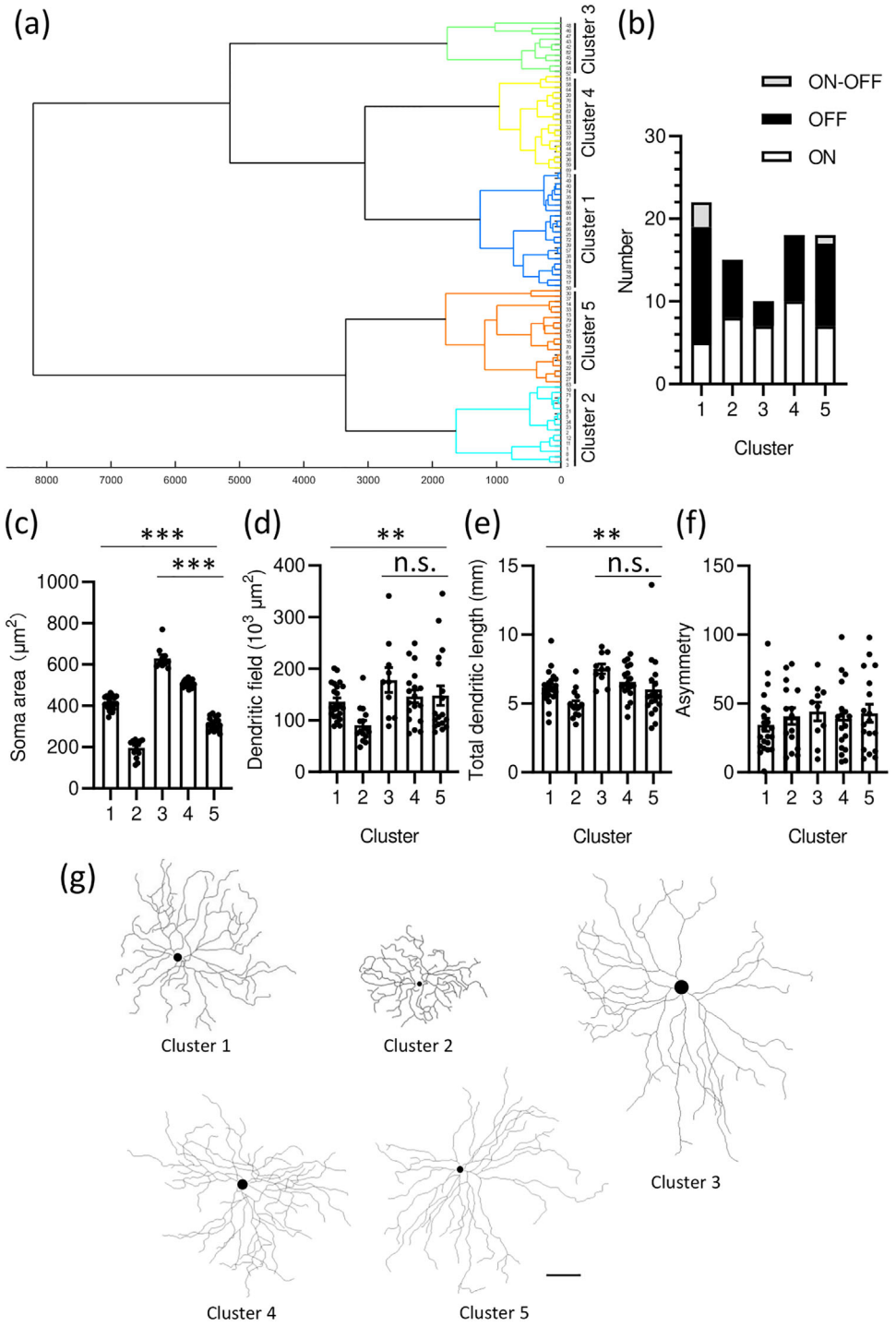

FIGURE 5 Classification of SMI-32+ RGCs into five clusters. (a) Hierarchical cluster analysis. (b) Number of cells in each cluster. (c) Soma area of all cells. (d) Dendritic field area of all cells. (e) Total dendritic length of all cells. (f): Arbor asymmetry of all cells (for all graphs, $n = 22$ for Cluster 1, $n = 15$ for cluster 2, $n = 10$ for cluster 3, $n = 18$ for cluster 4, $n = 18$ for cluster 5, one-way ANOVA, $^{*}p<.05$; $^{**}p<.01$; $^{***}p<.001$, data presented as mean ± SEM). (g) Representative cells in each cluster at the same magnification. Scale bar = 100 μm

3.6 | More than 90% of SMI-32^{+} RGCs were PV positive

It is known that other biomarkers label subsets of alpha RGCs in the mouse retina (Krieger et al., 2017). For example, PV covers more than 70% of alpha RGCs (Farrow et al., 2013; Munch et al., 2009), all transient OFF alpha RGCs are labeled by SMI-32 in calretinin (CB2) transgenic mice (Huberman et al., 2008), and melanopsin (Mel) stain sustained ON alpha RGCs (Estevez et al., 2012; Sonoda et al., 2020). To confirm this in the rat retina, we costained SMI-32 with PV (Figure 6a),

TABLE 3 Morphological parameters of each cluster

Cluster	*n*	ON, OFF			Soma area (mean ± SEM, μm²)	Dendritic field area (mean ± SEM, 10^3 μm²)	Total dendritic length (mean ± SEM, mm)
		ON	OFF	ON-OFF			
1	22	5	14	3	410.81 ± 6.77	136.10 ± 7.34	6.15 ± 0.25
2	15	8	7	–	196.15 ± 10.70	90.71 ± 8.80	4.95 ± 0.25
3	10	7	3	–	630.12 ± 17.58	177.94 ± 24.15	7.52 ± 0.35
4	18	10	8	–	570.82 ± 4.04	146.16 ± 12.25	6.57 ± 0.29
5	18	7	10	1	311.48 ± 7.50	147.83 ± 18.84	6.01 ± 0.55

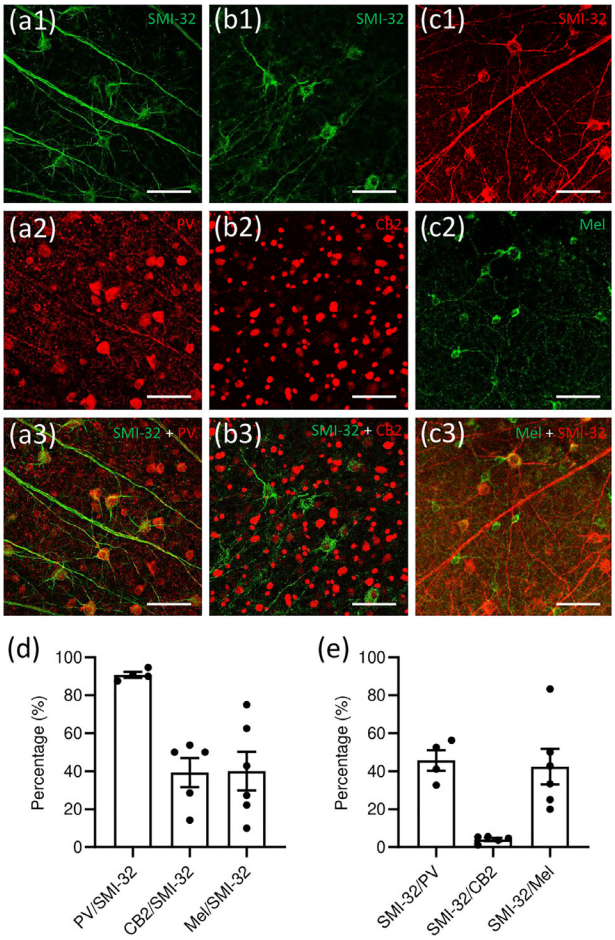

FIGURE 6 More than 90% of SMI-32⁺ RGCs were parvalbumin positive. (a) Costaining of SMI-32 (green) and PV (red), (b) costaining of SMI-32 (green) and CB2 (red), (c) costaining of SMI-32 (red) and Mel (green). (a–c) Scale bar = 100 μm. (d) Percentage of PV⁺, CB2⁺, Mel⁺, cells in SMI-32⁺ RGCs, (e) Percentage of SMI-32⁺ cells in PV⁺, CB2⁺, Mel⁺, RGCs (for all graphs, $n = 4$ for PV and SMI-32 costaining, $n = 5$ for CB2 and SMI-32 costaining, $n = 6$ for Mel and SMI-32 costaining; data presented as mean ± SEM)

CB2 (Figure 6b), and Mel (Figure 6c) and we found that more than 90% of SMI-32⁺ RGCs presented PV positive (PV/SMI-32: 90.78 ± 1.49%) (Figure 6d), which is a higher proportion than in the mouse retina (Farrow et al., 2013; Krieger et al., 2017; Munch et al., 2009). Similar proportions of SMI-32⁺ RGCs were costained with CB2 (CB2/SMI-32: 39.34 ± 7.68%) and Mel (Mel/SMI-32: 39.98 ± 10.19%) (Figure 6d). The proportion of SMI-32⁺ RGCs in PV, CB2, and Mel was also calculated; while there were similar proportions in PV and Mel, there was the least amount in CB2 (Figure 6e).

4 | DISCUSSION

4.1 | Distribution of SMI-32⁺ RGCs

SMI-32 antibodies were first generated to label cortical neurons (Ang et al., 1991; Campbell & Morrison, 1989; Sternberger & Sternberger, 1983), but they are now widely used to identify all populations of alpha RGCs (Bleckert et al., 2014; Krieger et al., 2017; Okigawa et al., 2020; Schmidt et al., 2014; Sonoda et al., 2020). The distribution of several SMI-32⁺ RGCs subsets has been studied in detail in rodents. Among these subsets, some are distributed evenly throughout the retina (Chan et al., 2011; Schmidt et al., 2014), while some are not (Bleckert et al., 2014; Sonoda et al., 2020). In humans, SMI-32⁺ RGCs are nonuniformly distributed across the retina, with a peak density of 100 cells/mm² at the center to 10 cells/mm² at the periphery (Straznicky et al., 1992). In our study, we calculated the entire population of SMI-32⁺ RGCs in all four quadrants (ST, IT, IN, SN), as well as in the central, middle, and peripheral retinal regions and found that SMI-32 RGCs were distributed evenly throughout the rat retina, with a density of approximately 130 cells/mm² (Figure 1).

4.2 | Morphology of SMI-32⁺ RGCs

The morphology of SMI-32⁺ RGCs, commonly thought to be similar to of alpha RGCs, has a large soma and dendritic field area and has relatively dense branched dendrites that rarely overlap (Peichl, 1989, 1991; Straznicky et al., 1992; Wassle et al., 1981a). Here, we filled a total of 83 SMI-32⁺ RGCs in the central, middle, and peripheral retinal regions with neurobiotin. The morphology of SMI-32⁺ RGCs in different retinal regions was investigated thoroughly, and comparisons between ON cells and OFF cells were made (Figures 2–4). We revealed that cells in different regions had distinct characteristics. Both the soma area (Figure 2e) and the dendritic field area (Figure 2f) were larger in ON cells than in OFF cells in the central retina, but not in

the middle or in the periphery. In OFF cells, the dendritic field area of the periphery was larger than at the center, but a pattern was not observed in ON cells (Figure 2f). Consistent with previous reports (Baden et al., 2016; Coombs et al., 2006), most of these SMI-32$^+$ RGCs had a large soma (≥20 μm), although a low percentage (11/83, 13.25%) had diameters smaller than 20 μm (Table 2). Arbor asymmetry analysis suggests that subsets of SMI-32$^+$ RGCs may have both symmetric and asymmetric arbor morphologies (Figure 3). Furthermore, we used Sholl analysis to describe the dendritic complexity of SMI-32$^+$ RGCs and revealed that SMI-32$^+$ ON cells and OFF cells have different dendritic structures, which perhaps reflect differences in physiological function (Figure 4).

4.3 | Classification of SMI-32$^+$ RGCs

With the development of imaging technology and the diversification of measurement dimensions, the classification of RGCs will become more and more precise in the future (Baden et al., 2016; Bae et al., 2018). From a functional perspective, it has been reported that SMI-32 labels four types of alpha RGCs, including ON-sustained, ON-transient, OFF-sustained, and OFF-transient (Krieger et al., 2017). In our study, we classified SMI-32$^+$ RGCs into five clusters based on morphology. Each cluster included both ON cells and OFF cells, indicating that cells that have different physiological functions may share similar morphology, which is consistent with previous work (van Wyk et al., 2009). One of these five clusters, which included ON and OFF cells, had small somas and a small dendritic field area. Cells in this cluster likely do not match the morphological characteristics of alpha RGCs (Figure 5). Based on this, combining morphological and physiological functions, SMI-32$^+$ RGCs may be grouped by a finer cluster classification. In addition, we found that PV and SMI-32 colabeled RGCs were predominant SMI-32$^+$ RGCs by more than 90% at the rat retinas (Figure 6d), which was much higher than the 70% reported in mice (Farrow et al., 2013; Krieger et al., 2017; Munch et al., 2009).

5 | CONCLUSIONS

In this study, using intracellular neurobiotin injections combined with SMI-32 antibody staining, we revealed that SMI-32$^+$ RGCs were distributed evenly throughout the rat retina, with a density of approximately 130 cells/mm^2. We compared morphological features of SMI-32$^+$ ON cells and OFF cells in the central, middle, and peripheral retinal regions and found that cells in different regions had distinct morphological characteristics. Most SMI-32$^+$ RGCs presented alpha-like cells with large somas and large dendritic field areas, but a small proportion of them had small somas and small dendritic fields. In addition, more than 90% of SMI-32$^+$ RGCs were colabeled with PV antibody.

ACKNOWLEDGMENTS

This work was supported by Key-Area Research and Development Program of Guangdong Province 2018B030331001 (to Liping Wang); National Natural Science Foundation of China 31930047 (to Liping Wang); Natural Science Foundation of Guangdong Province 2018A030313439 (to Wenshan Gui); National Natural Science Foundation of China 31630031 (to Liping Wang); Key Laboratory of Chinese Academy of Sciences 2019DP173024 (to Liping Wang).

AUTHOR CONTRIBUTIONS

Huiying Tan and Xiaotao Li designed the experiments. Huiying Tan and Xiaotao Li performed the experiments. Kang Huang and Moxuan Luo analyzed the data. Huiying Tan and Xiaotao Li drafted the manuscript. Liping Wang supervised all aspects of this project.

PEER REVIEW

The peer review history for this article is available at https://publons.com/publon/10.1002/cne.25275

DATA AVAILABILITY STATEMENT

The data used to support the findings of this study are available from the corresponding author upon request.

ORCID

Huiying Tan https://orcid.org/0000-0002-8680-7280

REFERENCES

Ang, L. C., Munoz, D. G., Shul, D., & George, D. H. (1991). SMI-32 immunoreactivity in human striate cortex during postnatal development. *Brain Research Developmental*, *61*(1), 103–109. https://doi.org/10.1016/0165-3806(91)90119-4

Baden, T., Berens, P., Franke, K., Roman Roson, M., Bethge, M., & Euler, T. (2016). The functional diversity of retinal ganglion cells in the mouse. *Nature*, *529*(7586), 345–350. https://doi.org/10.1038/nature16468

Bae, J. A., Mu, S., Kim, J. S., Turner, N. L., Tartavull, I., Kemnitz, N., Jordan, C. S., Norton, A. D., Silversmith, W. M., Prentki, R., Sorek, M., David, C., Jones, D. L., Bland, D., Sterling, A. L. R., Park, J., Briggman, K. L., Sebastian Seung, H., & Eyewirers. (2018). Digital museum of retinal ganglion cells with dense anatomy and physiology. *Cell*, *173*(5), 1293–1306 e1219. https://doi.org/10.1016/j.cell.2018.04.040

Bird, A. D., & Cuntz, H. (2019). Dissecting Sholl analysis into its functional components. *Cell Reports*, *27*(10), 3081–3096. https://doi.org/10.1016/j.celrep.2019.04.097

Bleckert, A., Schwartz, G. W., Turner, M. H., Rieke, F., & Wong, R. O. (2014). Visual space is represented by nonmatching topographies of distinct mouse retinal ganglion cell types. *Current Biology*, *24*(3), 310–315. https://doi.org/10.1016/j.cub.2013.12.020

Campbell, M. J., & Morrison, J. H. (1989). Monoclonal antibody to neurofilament protein (SMI-32) labels a subpopulation of pyramidal neurons in the human and monkey neocortex. *Journal of Comparative Neurology*, *282*(2), 191–205. https://doi.org/10.1002/cne.902820204

Chan, L. L., Lee, E. J., Humayun, M. S., & Weiland, J. D. (2011). Both electrical stimulation thresholds and SMI-32-immunoreactive retinal ganglion cell density correlate with age in S334ter line 3 rat retina. *Journal of Neurophysiology*, *105*(6), 2687–2697. https://doi.org/10.1152/jn.00619.2010

Condé, F., Lund, J. S., Jacobowitz, D. M., Baimbridge, K. G., & Lewis, D. A. (1994). Local circuit neurons immunoreactive for calretinin, calbindin D-28k or parvalbumin in monkey prefrontal cortex: Distribution and morphology. *Journal of Comparative Neurology*, *341*(1), 95–116. https://doi.org/10.1002/cne.903410109

Coombs, J., van der List, D., Wang, G. Y., & Chalupa, L. M. (2006). Morphological properties of mouse retinal ganglion cells. *Neuroscience*, *140*(1), 123–136. https://doi.org/10.1016/j.neuroscience.2006.02.079

Estevez, M. E., Fogerson, P. M., Ilardi, M. C., Borghuis, B. G., Chan, E., Weng, S., Auferkorte, O. N., Demb, J. B., & Berson, D. M. (2012). Form and function of the M4 cell, an intrinsically photosensitive retinal ganglion cell type contributing to geniculocortical vision. *Journal of Neuroscience*, *32*(39), 13608–13620. https://doi.org/10.1523/JNEUROSCI.1422-12.2012

Farrow, K., Teixeira, M., Szikra, T., Viney, T. J., Balint, K., Yonehara, K., & Roska, B. (2013). Ambient illumination toggles a neuronal circuit switch in the retina and visual perception at cone threshold. *Neuron*, *78*(2), 325–338. https://doi.org/10.1016/j.neuron.2013.02.014

Ferreira, T. A., Blackman, A. V., Oyrer, J., Jayabal, S., Chung, A. J., Watt, A. J., Sjöström, P. J., & van Meyel, D. J. (2014). Neuronal morphometry directly from bitmap images. *Nature Methods*, *11*(10), 982–984. https://doi.org/10.1038/nmeth.3125

Huberman, A. D., Manu, M., Koch, S. M., Susman, M. W., Lutz, A. B., Ullian, E. M., Baccus, S. A., & Barres, B. A. (2008). Architecture and activity-mediated refinement of axonal projections from a mosaic of genetically identified retinal ganglion cells. *Neuron*, *59*(3), 425–438. https://doi.org/10.1016/j.neuron.2008.07.018

Iaboni, D. S. M., Farrell, S. R., & Chauhan, B. C. (2020). Morphological multivariate cluster analysis of murine retinal ganglion cells selectively expressing yellow fluorescent protein. *Experimental Eye Research*, *196*, 108044. https://doi.org/10.1016/j.exer.2020.108044

Krieger, B., Qiao, M., Rousso, D. L., Sanes, J. R., & Meister, M. (2017). Four alpha ganglion cell types in mouse retina: Function, structure, and molecular signatures. *PLoS One*, *12*(7), e0180091. https://doi.org/10.1371/journal.pone.0180091

Lefebvre, J. L., Sanes, J. R., & Kay, J. N. (2015). Development of dendritic form and function. *Annual Review of Cell and Developmental Biology*, *31*, 741–777. https://doi.org/10.1146/annurev-cellbio-100913-013020

Lin, B., Wang, S. W., & Masland, R. H. (2004). Retinal ganglion cell type, size, and spacing can be specified independent of homotypic dendritic contacts. *Neuron*, *43*(4), 475–485. https://doi.org/10.1016/j.neuron.2004.08.002

Liu, J., & Sanes, J. R. (2017). Cellular and molecular analysis of dendritic morphogenesis in a retinal cell type that senses color contrast and ventral motion. *Journal of Neuroscience*, *37*(50), 12247–12262. https://doi.org/10.1523/JNEUROSCI.2098-17.2017

Munch, T. A., da Silveira, R. A., Siegert, S., Viney, T. J., Awatramani, G. B., & Roska, B. (2009). Approach sensitivity in the retina processed by a multifunctional neural circuit. *Nature Neuroscience*, *12*(10), 1308–1316. https://doi.org/10.1038/nn.2389

Okigawa, S., Yamaguchi, M., Ito, K. N., Takeuchi, R. F., Morimoto, N., & Osakada, F. (2020). Cell type- and layer-specific convergence in core and shell neurons of the dorsal lateral geniculate nucleus. *Journal of Comparative Neurology*, *529*, 2099–2124. https://doi.org/10.1002/cne.25075

Panda, S., Sato, T. K., Castrucci, A. M., Rollag, M. D., DeGrip, W. J., Hogenesch, J. B., Provencio, I., & Kay, S. A. (2002). Melanopsin (Opn4) requirement for normal light-induced circadian phase shifting. *Science*, *298*(5601), 2213–2216. https://doi.org/10.1126/science.1076848

Peichl, L. (1989). Alpha and delta ganglion cells in the rat retina. *Journal of Comparative Neurology*, *286*(1), 120–139. https://doi.org/10.1002/cne.902860108

Peichl, L. (1991). Alpha ganglion cells in mammalian retinae: Common properties, species differences, and some comments on other ganglion cells. *Visual Neuroscience*, *7*(1-2), 155–169. https://doi.org/10.1017/s0952523800011020

Peichl, L., & Wassle, H. (1981). Morphological identification of on- and off-centre brisk transient (Y) cells in the cat retina. *Proceedings of the Royal Society of London, Series B: Biological Sciences*, *212*(1187), 139–153. https://doi.org/10.1098/rspb.1981.0030

Ran, Y., Huang, Z., Baden, T., Schubert, T., Baayen, H., Berens, P., Franke, K., & Euler, T. (2020). Type-specific dendritic integration in mouse retinal ganglion cells. *Nature Communications*, *11*(1), 2101. https://doi.org/10.1038/s41467-020-15867-9

Schiffmann, S. N., Cheron, G., Lohof, A., d'Alcantara, P., Meyer, M., Parmentier, M., & Schurmans, S. (1999). Impaired motor coordination and Purkinje cell excitability in mice lacking calretinin. *Proceedings of the National Academy of Sciences of the United States of America*, *96*(9), 5257–5262. https://doi.org/10.1073/pnas.96.9.5257

Schmidt, T. M., Alam, N. M., Chen, S., Kofuji, P., Li, W., Prusky, G. T., & Hattar, S. (2014). A role for melanopsin in alpha retinal ganglion cells and contrast detection. *Neuron*, *82*(4), 781–788. https://doi.org/10.1016/j.neuron.2014.03.022

Sholl, D. A. (1953). Dendritic organization in the neurons of the visual and motor cortices of the cat. *Journal of Anatomy*, *87*(4), 387–406.

Sonoda, T., Okabe, Y., & Schmidt, T. M. (2020). Overlapping morphological and functional properties between M4 and M5 intrinsically photosensitive retinal ganglion cells. *Journal of Comparative Neurology*, *528*(6), 1028–1040. https://doi.org/10.1002/cne.24806

Sternberger, L. A., & Sternberger, N. H. (1983). Monoclonal antibodies distinguish phosphorylated and nonphosphorylated forms of neurofilaments in situ. *Proceedings of the National Academy of Sciences of the United States of America*, *80*(19), 6126–6130. https://doi.org/10.1073/pnas.80.19.6126

Straznicky, C., Vickers, J. C., Gábriel, R., & Costa, M. (1992). A neurofilament protein antibody selectively labels a large ganglion cell type in the human retina. *Brain Research*, *582*(1), 123–128. https://doi.org/10.1016/0006-8993(92)90325-4

van Wyk, M., Wassle, H., & Taylor, W. R. (2009). Receptive field properties of ON- and OFF-ganglion cells in the mouse retina. *Visual Neuroscience*, *26*(3), 297–308. https://doi.org/10.1017/S0952523809990137

Wassle, H., Peichl, L., & Boycott, B. B. (1981a). Morphology and topography of on- and off-alpha cells in the cat retina. *Proceedings of the Royal Society of London Series B Biological Sciences*, *212*(1187), 157–175. https://doi.org/10.1098/rspb.1981.0032

Wässle, H., Peichl, L., & Boycott, B. B. (1981b). Dendritic territories of cat retinal ganglion cells. *Nature*, *292*(5821), 344–345. https://doi.org/10.1038/292344a0

How to cite this article: Tan, H., Li, X., Huang, K., Luo, M., & Wang, L. (2022). Morphological and distributional properties of SMI-32 immunoreactive ganglion cells in the rat retina. *J Comp Neurol*, *530*, 1276–1287. https://doi.org/10.1002/cne.25275